J Fluoresc (2015) 25:59–68
DOI 10.1007/s10895-014-1479-8

ORIGINAL PAPER

Effect of Molecular-Level Insulation on the Performance of a Dye-Sensitized Solar Cell: Fluorescence Studies in Solid State

Na'il Saleh · Salah Al-Trawneh · Hmoud Al-Dmour · Samir Al-Taweel · John P. Graham

Received: 31 August 2014 / Accepted: 6 November 2014 / Published online: 16 November 2014

Abstract The performance of a dye-sensitized solar cell (DSSC) that is based on the host-guest encapsulation of 5-[4-diphenylamino)phenyl]thiophene-2-cyanoacrylic acid (**L1**) inside β-cyclodextrin hosts has been tested. The formation of the complex in the solid state and when adsorbed on TiO_2 was characterized using steady and picosecond time-resolved emission techniques, as well as time dependent DFT calculations. The molecular-level insulation has led to a small enhancement in the energy-conversion performance of the fabricated DSSC with the best results being an increase in the open circuit voltage (Voc) from 0.7 to 0.8 V. The importance of the present investigation lies in the unique spectroscopic characterizations of the examined materials in the solid state.

Keywords Triphenylamine · β-cyclodextrins · Time-resolved fluorescence spectroscopy · Solid state · Quantum calculations

Electronic supplementary material The online version of this article (doi:10.1007/s10895-014-1479-8) contains supplementary material, which is available to authorized users.

N. Saleh (✉) · J. P. Graham
Chemistry Department, College of Science, United Arab Emirates University, P.O. Box, 15551 Al-Ain, United Arab Emirates
e-mail: n.saleh@uaeu.ac.ae

S. Al-Trawneh · S. Al-Taweel
Chemistry Department, College of Science, Mu'tah University, Al-Karak, Jordan

H. Al-Dmour
Physics Department, College of Science, Mu'tah University, Al-Karak, Jordan

Introduction

The third generation photovoltaics cells, which are based on hybrid junction between inorganic nanocrystalline material and organic dye, so called dye sensitized solar cells (DSSCs), have the potential of low cost of fabrication and ease of production [1], which makes it a good candidate for commercialization. Recently, DSSCs efficiencies of 12.3 % have been attained using a zinc-porphyrin complex as a sensitizer along with a liquid electrolyte system [2], and efficiencies of 15 % for perovskite-based solid state DSSCs [3].

In the present investigation, we have selected 5-[4-diphenylamino)phenyl]thiophene-2-cyanoacrylic acid (**L1**) dye in Fig. 1 [4], whose structure contains donor-to-acceptor moieties bridged by a π-conjugated thiophene unit (so called, D–π–A molecular structure), where the triphenylamine (**TPA**) and cyanoacrylic acid moiety are the electron donor and electron acceptor/anchoring groups, respectively. While the use of **L1** dye has potential advantages in terms of improving electron injection from the excited dyes to the **TiO_2** surfaces [4], most of the fabricated cells that are based on **L1** suffered from low conversion efficiencies (η up to 4.55 % at most). The low efficiency was attributed to the strong intermolecular π–π interaction between the thiophene units, leading to dye aggregations, which decrease electron injection and enhance charge recombination of the injected electrons in **TiO_2** [5].

Several attempts to avoid dye aggregation and to get a more optimal performance for the DSSCs that are based on **L1** dye have been reported in literatures. These include, just to name a few, appropriate structural modifications on the π-conjugated thiophene units, such as inserting diphenyldibenzofulvene (**DPDBF**)-bridge between them [6], extending their linking [7], and linking alkyl groups to them [8]. Moreover, the reported structural modifications involved modifications on the **TPA** unit, such as inserting a bridge between the two phenyl rings [9], introducing bis-hexapropyltruxeneamino

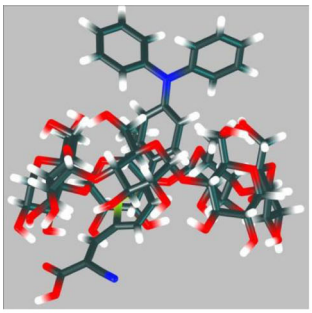

β-CD⊃L1 complex

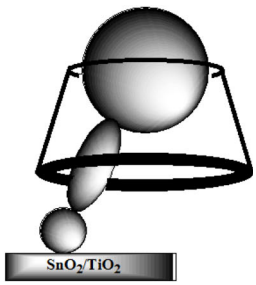

$SnO_2/TiO_2/$β-CD⊃L1

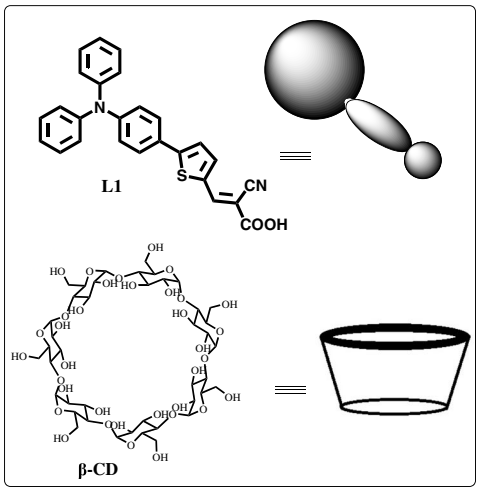

Fig. 1 The chemical structures for **L1** dye and the macrocycle host, **β-CD**. The proposed carbonic view of the resulted complex is also shown

units [10], substituting of hydrophobic hydrocarbons [11], and adding indoline units in which the work was conducted with or without adding some coadsorbents, such as **CDCA** (chenodeoxycholic acid) [12]. However, the best reported overall efficiency (η) in any of these studies has never exceeded 6.39 % [12].

The non-classical strategy adopted in the present work lies on the supramolecular encapsulation of an organic dye (**L1**) inside β-cyclodextrin (**β-CD**) (Fig. 1), and the subsequent adsorption on the $\mathbf{TiO_2}$ surface. **β-CD** is composed of seven glucopyranose subunits that make-up a ring with a conical cylinder structure (Fig. 1). The non-covalent encapsulation should prevent the self-aggregation of the dyes and retard the interfacial charge recombination dynamics, thus enhancing the device power conversion. Although, the influence of dye/cyclodextrin host-guest systems on DSSC performance is known (see Discussion below), recording cell efficiencies over 4 %, the present study focuses on characterizing the spectroscopic and photophysics of **L1** molecules in the solid state (not in solution [13]) before and after adsorption on the titanium oxide nanoparticles using stationary and time-resolved measurements methods, which has not been realized in literature to the best of our knowledge.

In short, we have encapsulated **L1** inside **β-CD** cavity in solid state and characterized the products using steady and picoseconds time-resolved emission techniques. The solar conversion performance of the fabricated DSSC from **L1** was compared before and after mixing with **β-CD** and the results demonstrated small enhancement in solar cells efficiencies.

Experimental Section

Synthesis of **L1** Dye

All chemicals from Sigma-Aldrich were purchased and used without further purification. Methylformamide was purchased from Acros. The silica gel for column chromatography was purchased from Macherew-Nagel GmbH & Co.KG (Germany). Melting point was determined on a scientific melting point apparatus in open-capillary tubes. ^{1}H-NMR spectra were recorded on 400 MHz spectrometer on Bruker Avance III (100 MHz for ^{13}H-NMR) with TMS as the internal standard for solution in DMSO-d_6.

*Synthesis of 5–[4-(Diphenylamino)Phenyl] Thiophene-2-Carbaldehyde (**1**)*

To a solution of 4-bromo-N,N-diphenylaniline (0.58 g, 1.8 mmole) and $PdCl_2$ (Ph_3P) (0.10 g, 1.2 mmole) in dry DMF (10 ml) was added 5-formylthiophene-2-yl-2-boronic acid (0.30 g, 1.92 mmole) and Na_2CO_3 (0.60 g, 5.6 mmole). The reaction mixture was heated at 100 °C for 24 h under N_2 atmosphere (Fig. 2). The reaction mixture was quenched by the addition of water (30 ml) to produce black gum precipitate, which was filtered, then dissolved in $CHCl_3$ (40 ml), dried over anhydrous magnesium sulfate to produce 0.6 g of black to green semi-solid which was purified with Column Chromatography over silica gel using a 1:1 hexane/dichloromethane as the eluent. Yellow fraction was collected to produce a bright yellow powder 0.30 g, 50 % yield, with a melting point of 99–102 °C.

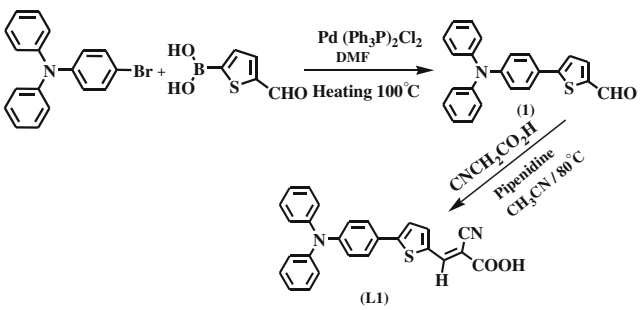

Fig. 2 Preparation of 5-[4-(diphenyl amino)phenyl]thiophene-2-cyanoacrylic acid (**L1**) dye

*Synthesis of 5-[4-Diphenylamino)Phenyl] Thiophene-2-Cyanoacrylic Acid (***L1***)*

A 20 ml acetontrile solution of 5 −[4-(Diphenylamino)phenyl] thiophene-2-carbaldehyde **(1)** (0.30 g , 0.9 mmole), cyanoacetic acid (0.4 g, 4.7 mmole), and piperidine (1 ml) was refluxed for 16 h under nitrogen atmosphere (Fig. 2). The reaction mixture was added to petroleum ether (15 ml) and HCl (15 ml, 0.1 M), a dark violet precipitate was formed, this precipitate was filtered to yield (**L1**) (0.3 g, 80 %) with a melting point of 212–215 °C. The NMR data (See Figures S1 to S4 in the Supporting Information) were in according to the literature [4], as follows: ^{13}C- NMR (DMSO-d_6/ 100 MHz), δ (ppm)=97.3 (C-15); 116.6 (C-17, -CN); 121.6 (C-8); 123.9 (C-3); 124.1 (C-13); 125.0 (C-11); 125.3 (C-4); 127.4 (C-7); 129.7 (C-12); 133.5 (C-6); 141.7 (C- 5); 146.3 (C-10); 146.5 (C-9); 148.6 (C-2); 153.2 (C-14); 163.7 (C-16, -COOH), ^{1}H-NMR (DMSO-d_6/ 400 MHz), δ (ppm)=6.96 (^3J=8.8Hz, 2H, H-8); 7.09 (^3J=7.6Hz, 4H, H-11); 7.13 (^3J=7.2Hz, 2H, H-13); 7.35 (^3J=7.6Hz, 4H, H-12); 7.62 (^3J=4 Hz, 1H, H-4), 7.66 (^3J=8.8Hz, 2H, H-7); 7.98 (^3J=4 Hz, 1H, H-3); 8.46 (s, 1H, H-14); 8.72 (br, 1H, −COO*H*). Also, High resolution mass spectroscopy (HRMS) for **L1** gave $[M+H]^+$= 423.11655, Calculated=423.11617

Absorption and Steady-State Fluorescence Measurements

All absorption and fluorescence measurements were performed on solutions in 1 cm^2 quartz cuvettes. The fluorescence data in the solid state were collected using a 0.5-mm demountable cuvette to maintain front-face excitation geometry. Absorption spectra were measured using Cary-300 UV–vis spectrophotometer, while fluorescence spectra were measured on Cary-Eclipse spectrometer with a slit width of 5 nm for both the excitation and emission wavelengths in solution. The binding constants were calculated by using the classical titration method in which the concentrations of the guest were kept constant while changing the amount of added host macrocycles. The difference in absorbance of **L1** in the presence and absence of **β-CD** was measured at selected wavelength (in which variation is as large as possible), and the data was plotted against the concentration of the host. The data in the inset of Figure S5 (Supporting Information) were fitted to a nonlinear formula previously reported [14] using the Marquette algorithms provide by SigmaPlot software. All solutions of **L1** were made in ethanol-water solution (1:10, v/v). The water used was doubly distilled and deionizied (conductivity less than 0.05 μS), and the ethanol solvent was of spectroscopic grade. The stationary fluorescence measurements in solutions were carried out at **L1** concentration of 10×10^{-6} M.

Picoseconds, Time-Resolved Fluorescence Measurements

The fluorescence lifetimes were measured by time-correlated single-photon counting (TCSPC) on LifeSpec II spectrometer (Edinburgh Instruments) by using EPL-375 picosecond pulsed diode laser (λ_{ex}=375 nm, repetition rate=5 MHz) for excitation; and monitored emission maxima at 560 nm or 600 nm. The time-resolved emission (intensity of ~1000–3000 counts/s) was collected (up to 10,000 counts/s) by a red-sensitive high speed PMT (Hamamatsu, H5773-04) detector. And, the data were analyzed by the iterative reconvolution method using the instrument's software that utilizes the Marquardt-Levenberg algorithm to minimize χ^2. A typical instrument response function (IRF) of *ca.* 30 ps (*fwhm*) was confirmed after numerical reconvolution. The fluorescence lifetimes in the solid state were collected using a 0.5-mm demountable cuvette to maintain front-face excitation geometry. We believe that in our experimental conditions the observed emission is fully dominated by the fluorescence from the fluorophore in question. The fluorescence decay was analyzed in terms of the multiexponential model: $I(t) = \sum_i \alpha_i exp(-t/\tau_i)$,where τ_i are the lifetimes with amplitudes α_i and α_i=1.0. The contribution of each component to the steady-state intensity is given by: $f_i = \frac{\alpha_i\tau_i}{\sum_j \alpha_j\tau_j}$,where the sum in the denominator is over all the decay times and amplitudes. The mean decay time (average lifetime) is given by: $\overline{\tau} = \sum_i f_i\tau_i$. The amplitude-weighted lifetime is given by: $\langle\tau\rangle = \sum_i \alpha_i\tau_i$.

Host-Guest Complex Formation in Solid State and Adsorption Experiments

Stable thin films of the new solid complex **β-CD⊃L1** were formed readily upon mixing the host and guest molecules. First, an equivalent amount of **L1** and **β-CD** (3 mM) were added into ethanol-water solution (1:10, v/v) aqueous solutions, and the resulted suspension was filtrated following vigorous sonication and vortexes using a PTFE filter membrane. Then, a vacuum evaporation was implemented to fabricate a thin film of the **β-CD⊃L1** solid complex directly on the top of the demountable cuvette which was mounted by the front-face holder.

SnO_2/TiO_2/β-CD⊃L1 was prepared through soaking the **SnO_2/TiO_2** electrodes in the **β-CD** solution with concentration of 0.8 mM in pure H_2O in according to the reported procedure by others [15]. The slide was then kept at room temperature for 12 h to absorb the dye. During this time the container was covered with aluminum foil to prevent light from bleaching the dye. The substrate was removed from the solution using tweezers and rinsed in methanol immediately. Then, the **β-CD/TiO_2** film was dried under a nitrogen flow for 3 min. In the second step, the resulted film was washed in absolute ethanol and dried by vacuum before it was immersed

into **L1** solution in ethanol (0.3 mM) and kept at room temperature for 4 h. **SnO_2/TiO_2/β-CD** and **SnO_2/TiO_2/L1** were also prepared using a similar procedures. The **β-CD** hosts were purchased from Sigma-Aldrich and used without further purifications. Prior to preparing the dye solution, a vial was cleaned with Decon 90® and rinsed in hot water and the ultrapure water, and dried under a stream of warm air for 5 min.

Computational Details

The ADF 2012 [16, 17] and Gaussian 09 [18] programs were used for all calculations. The structure of the free **L1** ligand was optimized using Gaussian 09 and the B3LYP [19–22] functional and 6–311+G(d,p) basis set in the ground state. Time dependent DFT calculations using the CAM-B3LYP functional [23] and 6–311+G(d,p) basis set were used to calculate the electronic spectrum of **L1** and the geometry of the first excited state. To determine possible structures of the inclusion complex of **L1** with **β-CD**, initial geometry optimization calculations were performed using Gaussian 09 and the ONIOM method [24], employing PM3 calculations for the **β-CD** and B3LYP/6-31G(d) for the **L1** ligand. Various starting geometries were used to determine optimal orientation of the **L1** ligand within the **β-CD** cavity. The lowest energy of these were then further optimized using ADF and the BLYP-D dispersion [25] corrected functional and DZP (double-zeta with polarization functions) basis set. Following full optimization, single point calculations were performed using BLYP-D/TZP to determine total energy and orbital energies and isosurfaces.

Construction and Characteristics of Solar Cells Based on the TiO_2 Semiconducting Polymer Heterojunction

The devices studied here were fabricated on fluorine-doped, tin oxide (**SnO_2:F**) electrodes, pre-coated with a thin, dense layer of **TiO_2**. A TiO_2 sol-gel (Ti-Nanoxide T) was then spread over the substrates using a doctor blade and cured to form the anatase phase following the procedures described in [26]. Typically, the resulting porous, **TiO_2** layer was ~2 μm. **SnO_2/TiO_2/ β-CD⊃L1** film was prepared through soaking the **SnO_2/TiO_2** electrodes in the **β-CD** and the dye solutions (see above). A drop of poly(3-hexylthiophene) polymer (**P3HT**) in chloroform (15 mg/mL) was allowed to suffuse into this layer for several seconds prior to spincoating at 1000 rpm. The devices were completed by evaporating an array of 3 mm^2, circular gold electrodes onto the **P3HT**.

Electrical Characterization

Current-voltage (I-V) characteristics were measured using a Keithley Model 237 High-Voltage Source-Measure Unit in dark and light. The optical response of the solar cells was obtained using a Full Spectrum Solar Simulator (150 W Xenon Lamp). To limit the light to the region defined by the gold top electrode, a mask with identical holes (size and distribution of holes are fixed) was placed against the glass substrate. The light intensity was measured using a light intensity meter. A light intensity equivalent to AM1.5 radiation from Xenon lamp was set using Reference solar cell and meter.

Results

Spectral and Photophysical Properties in the Solid State

The spectral and photophysical properties of triphenylamine derivatives were examined in literature [27, 12]. Figure S5 and Figure S6 in the Supporting Information represents the UV −vis absorption spectra of **L1** dye in the presence and absence of host molecules in ethanol-water solution (1:10, v/v) and when adsorbed on **TiO_2** surfaces, respectively. In the visible range, **L1** shows a typical and a strong absorption band located at 428 nm, which arises from the intramolecular charge transfer (**ICT**) between the donor and the acceptor moieties [27]. In the UV region, the absorption around 300 nm is known to originate from a π-π* transition.

The emission spectra for free and **β-CD**-bound **L1** in the solid state are shown in Fig. 3a. The emission maximum was blue-shifted (by 137 nm) from 678 nm to 541 nm upon the formation of inclusion complex **β-CD⊃L1**. Moreover, the emission decays recorded in the presence and absence of the host molecules in the solid state at 560 nm and 600 nm wavelengths of observation, respectively, upon excitation at 375 nm (30 picoseconds time-resolution) in Fig. 3b, revealed a ~6-fold enhancement in the average and amplitude-weighted fluorescence lifetime from 330 ps to 1851 ps and from 222 ps to 1648 ps, respectively. Table 1 presents the extracted data from the biexponential fits. The results are rationalized by the confinement effects rather than the polarity effects of the encapsulation process (see theoretical results). In order to assign the double exponential decays, the time-resolved emission spectra (**TRES**) in the solid state in Fig. 3c and d were conducted. While the two decay components of the excited **L1** dye at 130 ps and 484 ps are associated with an **ICT** state that probably decays with biexponential kinetics, the other two at 370 ps and 1.9 ns arise from two different forms of the **β-CD⊃L1** complex with the nanosecond-emission component has its band at the red-side of the spectrum (560 nm vs. 520 nm), in agreement with the theoretical results below. Thus, the complex has formed completely in the solid state. The steady fluorescence spectra for the dye and the host compounds when adsorbed on the **TiO_2** slides showed some

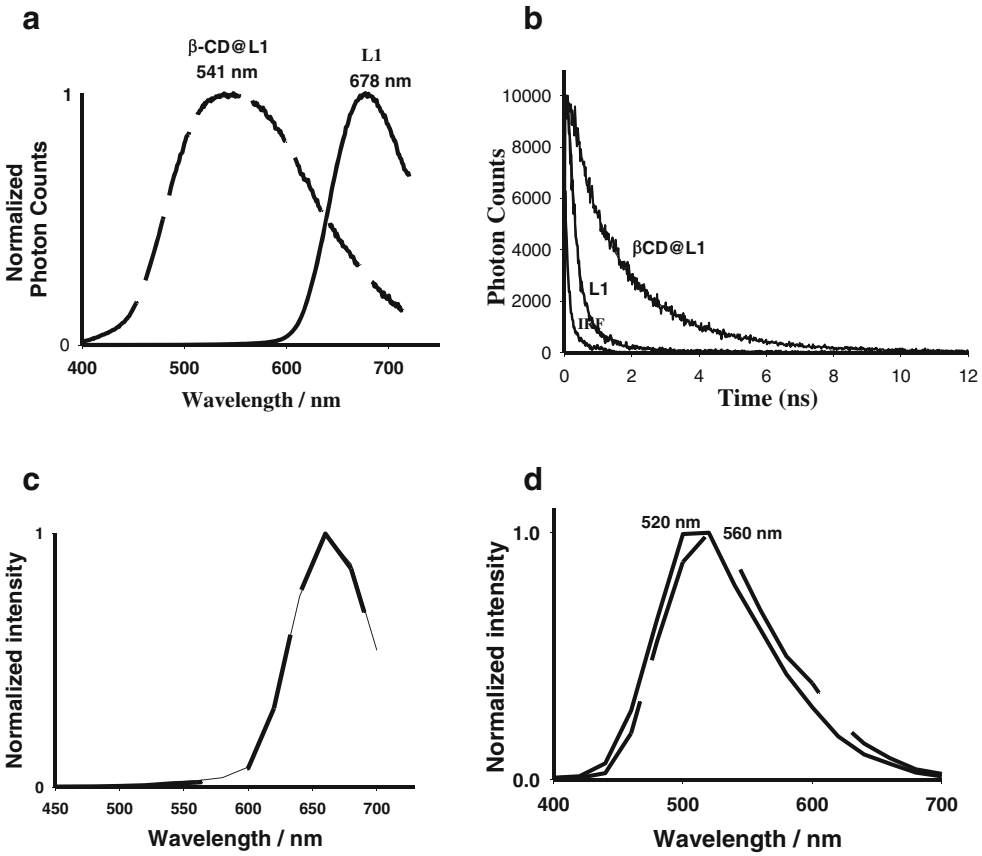

Fig. 3 The emission spectra of **L1** (*solid line*) and **β-CD⊃L1** (*dashed line*) (**a**). Lifetime traces of **L1** and **β-CD⊃L1** (**b**), and time-resolved emission spectra (**TRES**) of **L1** (**c**) and **β-CD⊃L1** (D) gated at 200 ps (*solid lines*) and 2 ns (*dashed lines*). Fluorescence intensity has been normalized. Measurements in the solid-state were investigated at 298 K and λ_{ex}=375 nm with instrument response function (IRF) of *ca.* 30 ps (*fwhm*)

blue shift of the peak position from 630 to 600 nm upon the addition of **β-CD** (Figure S7). This means, the extent of encapsulation is less than what is observed in the isolated solid state.

Theoretical Characterizations

Time Dependent DFT calculations using the CAM-B3LYP functional and 6–311+G(d,p) basis set predict absorption wavelengths of 404 nm for the **ICT** transition and 270 nm for the π-π* transition.

Possible structures for encapsulation complexes were investigated using the ONIOM method with PM3 calculations for **β-CD** and the B3LYP functional and 6-31G(d) basis set for **L1**. Several possible orientations of **L1** within the cyclodextrin cavity were investigated and the lowest energy of these was further optimized using the ADF program and dispersion corrected BLYP-D functional. The structures were reoptimized with a double-ζ basis set with polarization functions for all atoms. Following optimization, total energies and molecular orbital energies were calculated using a triple-ζ basis set with polarization functions. In each case it was found that encapsulation of **L1** within the **β-CD** cavity did not result

Table 1 Spectroscopic and photophysical data (λ_{ex}=375 nm) of **L1** in the absence and presence of **β-CD** in the solid state

Sample	λ_{abs}/ nm	λ_{em}/ nm	λ_{obs}/ nm	α_i	τ_i (ps)	$\langle\tau\rangle$ (ps)	f_i	$\bar{\tau}$ (ps)	χ^2
L1	429	678	600	0.74 0.26	130 484	222	0.44 0.56	330	1.08
β-CD⊃L1	430	541	560	0.17 0.83	370 1910	1648	0.040 0.96	1851	0.971

The excitation was 375 nm and instrument response function (IRF) of *ca.* 30 ps (*fwhm*)

$$\bar{\tau} = \sum_i f_i \tau_i f_i = \frac{\alpha_i \tau_i}{\sum_j \alpha_j \tau_j}$$
$$\langle\tau\rangle = \sum_i \alpha_i \tau_i$$

χ^2 values for double-exponential fit

Table 2 Relative total energies and HOMO & LUMO energies for **L1** and inclusion complexes **β-CD⊃L1**

	Relative total energy (kJ/mole)	HOMO (eV)	LUMO (eV)
L1 free ligand	***	−4.73	−3.27
Inclusion complex 1	0.0	−4.79	−3.35
Inclusion complex 2	+23.4	−4.69	−3.55

in a large change in frontier orbital energies. Table 2 below summarizes the orbital energies for the free ligand and the two lowest energy encapsulation complexes: The relatively small shifts in HOMO and LUMO energies on encapsulation can be understood for the spatial distribution of the frontier orbitals: As shown in Fig. 4 below, the HOMO and LUMO of **L1** lie largely localized outside of the cyclodextrin cavity. It is consequently suggested that changes in fluorescence of **L1** upon encapsulation result largely from confinement rather than polarity effects: Time-dependent DFT geometry optimization of the S_1 state of **L1** shows that the first excited state of **L1** is considerably more planar than the ground state, and the large change in geometry allows for significant Stoke's shift. Encapsulation may prevent the rearrangement of the ligand in the S_1 state, resulting in a smaller Stoke's shift and longer lifetime. However, we were unable to complete TDDFT geometry optimization of the encapsulation complex to verify this explanation due to the excessive computational cost of such a calculation.

Structural Characteristics of the Constructed DSSC

Figure S8 shows the XRD signal of **TiO_2** films in the present study. We observed a strong diffraction peak which occurred at a Bragg angle of $2\theta \sim 25^0$, while smaller peaks were observed near 48° and 54° and corresponded to reflections from the 101, 200, and 105 lattice planes of the particles. These lattice planes occur in a tetragonal system and correspond to the anatase phase of **TiO_2**. To determine the grain size, the Schreer equation was applied to the largest diffraction peak

$$GS = \frac{k\lambda}{\beta cos\theta} \quad (1)$$

where λ=0.15 nm is the X-Ray wavelength, GS is the grain size and β is the full width at half maximum of the diffraction peak. From Figure S8, the largest peak occurs at 2θ=25.1° for the reflection from the 101 lattice plane. Substituting the following values in Eq. (1), 1: β=0.00416 radians, cos 12.55=0.97 and K=0.96, the grain size is estimated to be 36 nm. Figure S9 shows the cross section of **SnO_2:Fn/compact TiO_2/nc-TiO_2** thin film. From the image, the layer is estimated to be ~1.7 μm. This value might be a slight difference around 300 nm than what we have expected due to the lack of uniform thickness of **nc-TiO_2** by using doctor blade technique. For the particles size, Figure S9 also shows the top view of **SnO_2:Fn/compact TiO_2/nc-TiO_2** thin film. It is revealed that the particle size is between 20 and 25 nm. It is also evident that the particles are distributed over the surface of **nc-TiO_2** with pin holes. To achieve better performance solar cells, one needs to improve the penetration of dye and polymer though the pin holes.

Electrical Characteristics of the Constructed DSSC

The three and double layer solar cells (**TLSC** and **DLSC**) were fabricated using an organic semiconductor instead of the electrolyte in Ko Cell [15]. The current density–voltage (J-V) characteristics for these devices were measured in the dark and under solar simulator. In additions to that, the external quantum efficiency of our solar cells was measured to compare between them. The effects of encapsulation dyes with host on the solar cell parameters were investigated. Figure 5a shows the current density-voltage (J-V) characteristics of a typical **TLSC** (for **L1** dye) in linear and semilog form, respectively. In the dark, the devices displayed good diode characteristics. In the present case, the forward current, turned on at ~0.7 V and by 1 V, had risen to ~0.05 mA/cm^2. At -1 V the reverse current was 0.00034 mA/cm^2, giving a rectification ratio of 500. Under illumination, the device displayed good solar cells characteristics with the current short circuit current density (Jsc) of 0.08 mA/cm^{-2}, open circuit voltage (Voc) of 0.7 V, and fill factor of 44 %, yielding power conversion efficiency (μ) of 0.027 %. The effects of supramolecular encapsulation of the triphenylamine dye (**L1**) on the parameters of **TLSC** were investigated. Figure 4b shows the current-voltage characteristics of the devices fabricated from **L1** encapsulated with **β-CD**. As seen, the Voc of the encapsulated device increased by ~0.1 V in comparison with the devices without **β-CD**. These results were similar to the work done by Grtazel Group

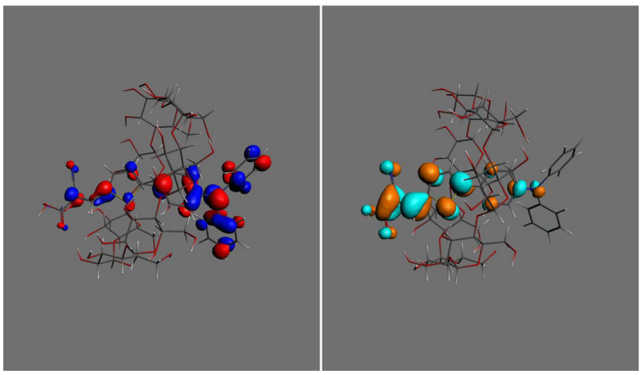

Fig. 4 HOMO and LUMO isosurfaces for inclusion complex 1

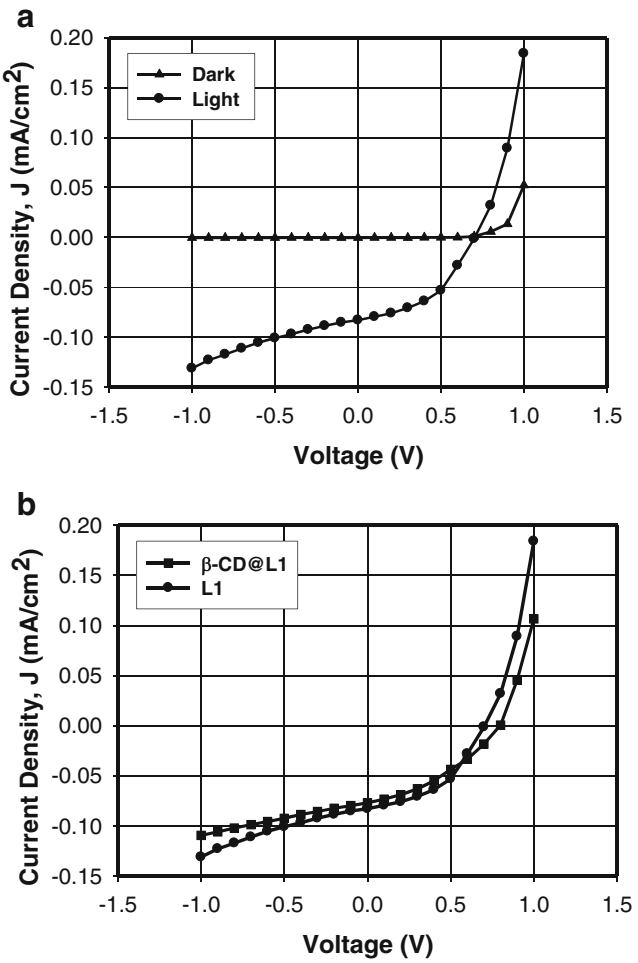

Fig. 5 J-V characteristics of a typical TLSC produced from **L1** dye on TiO_2 (**a**); and from **L1** encapsulated on TiO_2 with **β-CD** (**b**)

[15]. The Voc improved by around 0.07 V, which was lower than the Voc of our device. On contrary to our findings, the short circuit current improved by around 3 % for Grtazel device upon encapsulation, while our short circuit current did not change a lot upon encapsulation. Table 3 shows summary of the parameters of solar cells that is based on dye **L1** before and after complexation with **β-CD**.

Table 3 Comparison of parameter of solar cells produced from free and **β-CD**-bound **L1** dye

Parameter	SnO_2/TiO_2/ βCD⊃L1/P3HT/Au	SnO_2/TiO_2/ L1/P3HT/Au
Open circuit voltage (Voc)	0.8	0.7
Short circuit current density, Jsc (mA/cm^2)	0.078	0.082
Fill factor %	36 %	44 %
Power conversion efficiency (μ %)	0.024 %	0.025 %

Discussion

The solar cells in this work were fabricated with the aim of producing an efficient energy by converting an eco-friendly, cheap, abundant materials onto more beneficial and mechanistic molecular tools using simple and straightforward methods. The novelty of the method used lies on the utilization of non-covalent interactions in constructing bulk materials that perform useful functions in solar cell technology. The study aimed at evaluating the effect of supramolecular strategy on the performance of DSSC cells that was fabricated from a host-guest complex between **L1** and **β-CD** with the goal of preventing dye aggregations instead of the classical structural modifications of the organic dye.

The simplest configuration of DSSC is to have the organic material sandwiched between two electrodes of different work functions. Figure S10 and S11 illustrate the steps involved in the operation of DSSC [5]. The system comprises a dye that is bound to the surface of **nc-TiO_2**, which provides a large surface area to which the dye could be adsorbed. This is crucial for efficient light harvesting. The porous **TiO_2** layer is interpenetrated by a hole-transport material (**HTM**), such as **P3HT** in this work. Excitation of the dye should lead to the injection of electrons from the excited dye to the conduction band of the **TiO_2**. The ground state of the dye will then be regenerated through reduction by the **HTM** to give the required charge separation. Charges will migrate and be collected at a transparent conducting electrode (e.g., **SnO_2** and **Au** electrode).

The dyes used in DSSC technology must conform to a number of essential design requirements in order to function. They must bind strongly to **TiO_2** by means of an anchoring group, typically carboxylic or phosphonic acid groups, to ensure efficient electron injection (k_1) into the **TiO_2** conducting band and to prevent gradual leaching by the electrolyte. The LUMO of the dye must be sufficiently high in energy for efficient charge injection into the **TiO_2**, and the HOMO must sufficiently be low in energy for efficient regeneration of the oxidized dye by the **HTM** (Figure S11). The dye must absorb solar radiation strongly with absorption bands in the visible or near-IR region, preferably covering a broad range of wavelengths. Electron transfer from the dye to the **TiO_2** must also be rapid in comparison with decay to the ground state of the dye.

Here, the supramolecular encapsulation of an organic dye (**L1**) inside **β-CD**, and the subsequent adsorption on **nc-TiO_2** surface, was expected to enhance redox reversibility, electroluminescent efficiency, thermal stability and photochemical stability [28]. One could also speculate an increase in cell efficiency due to the employed host-guest complex since the addition of macromolecules should (*i*) prevent the aggregations of the dyes, thus suppressing deactivation of the excited state of the dye (k_7) [29, 30], (*ii*) prevent the interaction

between **HTM** and the **TiO_2** surface, thus minimizing k_5 loss [5], (*iii*) increase physical separation of the cationic dye from the **TiO_2** [31], thus suppressing significantly the rate for k_6 [32], (*iv*) improve long-term stability against water-desorption, as well as thermal [15] and photochemical stability as reported on other systems [33, 30, 34], (*v*) promote charge-transfer cascades between the dye and **HTM**, which should lead to a stronger electronic communication and faster regeneration kinetics (k_2) of the dye [35], and (*vi*) enhance the fluorescence lifetimes of the dye while encapsulated in the host, thus minimizing the deactivation of the excited state of the dye (k_7) [36, 37, 29].

Several studies have used **CD** macrocycles to prevent aggregation of the dyes [38–40, 15, 32]. Haque *et al.*, studied an azobenzene dye encapsulated within **α-CD** molecule and attached to TiO_2 [32]. The hydrophilic outer layer of the **α-CD** was found to be suitable for adsorption onto the **TiO_2** surface. The hydrophobic inner surface, on the contrary, was found to be suitable for the spatial separation of the dye from the **TiO_2**, suppressing significantly the rate for k_6 and offering potential gains in cell efficiency. Yeow et al., studied the effects of encapsulation of a dye molecules by cucurbit [7]uril (**CB7**) on the charge-recombination dynamics [41]. Comparison of the so-called "emission intensity time traces" of the free and **CB7**-bound dye revealed that encapsulation inside **CB7** reduced the rate for k_6, thus suppressing the loss mechanism. More recently, Ko et al. [15] encapsulated other dyes with **TPA** and cyanoacetic acid moieties inside various **CD** cavities (**α-CD**, **β-CD**, and **γ-CD**) and obtained using a polymer gel electrolyte an overall conversion efficiency of 7.4 %. Also, they found the new **CD**-based device to have excellent stability under light soaking at 60 °C for 1000 h. They attributed the high efficiency and excellent stability to the encapsulation of their dye inside the **CD** cavity. Thus, the non-covalent interactions despites being weak forces (e.g., ion-dipole forces and hydrogen bonding), they were sufficient to improve the cell efficiency [15, 32, 41].

Nevertheless, the small improvement in our case could be rationalized by the inherent competitive displacement of the dye from the cavity of the host through the more thermodynamically favored covalent anchoring on the surface. For example, the calculated complexation percentage from the binding constant (Figure S5) and the concentration of the free and host molecules was only 60 %.

The theoretical calculations also support the experimental measurements. To promote efficient charge injection (k_1) and dye regeneration (k_2) in the **DSSC**, the LUMO must remain sufficiently higher than the edge of the conduction band of **TiO_2** for efficient charge injection while the HOMO must remain sufficiently below the redox level of the **HTM** for efficient regeneration of the dye (Figure S11) [42, 43]. The theoretical results here demonstrated that such energy lying was not significantly alerted in the presence of the macrocyclic **β-CD** host, with the energy of the HOMO changing by +0.04 to −0.07 eV and energy of the LUMO changing by −0.13 to −0.28 eV in the optimized structures for inclusion complexes, leading to a small increase the Voc of encapsulated dye solar cells from 0.7 to 0.8 V (Table 3).

The solar cell device produced low light current even after the dye is encapsulated because there is not sufficient force to separate holes–electrons pair formed at interface and hole are not hopping easily from dye to **P3HT** and electron from dye to **nc-TiO_2**, causing an increase in the decay of exciton by recombining the electrons with hole on the sits of dyes.

Conclusion and Future Work

The complex formation between 5-[4-diphenylamino)phenyl]thiophene-2-cyanoacrylic acid (**L1**) dye and β-cyclodextrin hosts has been characterized using steady and ultrafast spectroscopic methods in the solid state, as well as by DFT calculations. The effect of such molecular insulation on the performance of the fabricated dye-sensitized solar cells (DSSCs) has been evaluated, indicating a weak enhancement of the solar cell efficiency.

The results reported by the group of Yeow on the inclusion of dye molecules into CB7, implied that a strong encapsulation of the dye is essential in order to avoid fast charge recombination. As the binding constant reported here is comparable to that reported by Yeow [41] (9100 versus 2290 for the dye reported by Yeow group [41]), our results are not a surprise and as such more pronounced effects of supramolecular systems are expected with a much higher affinity between the guest and the host that could sustain the competing processes during the adsorption step of the dyes on **TiO_2** surfaces.

Acknowledgments The authors wish to thank the Scientific Research Support Fund in Jordan under the program SRF 2010/07/01. N.S. thanks the research program at United Arab Emirates University for their financial support 27/11/2.

References

1. Oregan B, Gratzel M (1991) A low-cost, high-efficiency solar-cell based on dye-sensitized colloidal TiO_2 films. Nature 353(6346):737–740
2. Yella A, Lee H-W, Tsao HN, Yi C, Chandiran AK, Nazeeruddin MK, Diau EW-G, Yeh C-Y, Zakeeruddin SM, Graetzel M (2011) Porphyrin-sensitized solar cells with cobalt (II/III)-based redox electrolyte exceed 12 percent efficiency. Science 334(6056):629–634
3. Burschka J, Pellet N, Moon S-J, Humphry-Baker R, Gao P, Nazeeruddin MK, Graetzel M (2013) Sequential deposition as a route to high-performance perovskite-sensitized solar cells. Nature 499(7458):316–319
4. Hagberg DP, Marinado T, Karlsson KM, Nonomura K, Qin P, Boschloo G, Brinck T, Hagfeldt A, Sun L (2007) Tuning the

HOMO and LUMO energy levels of organic chromophores for dye sensitized solar cells. J Org Chem 72(25):9550–9556
5. Robertson N (2006) Optimizing dyes for dye-sensitized solar cells. Angew Chem Int Ed 45(15):2338–2345
6. Li H, Tang R, Hou Y, Yang Y, Chen J, Liu L, Han H, Peng T, Li Q, Li Z (2014) Diphenyldibenzofulvene-based sensitizers for efficient dye-sensitized solar cells: the tuned absorption properties and partially suppressed aggregation. Asian J Org Chem 3(2):176–184
7. Ciofini I, Le Bahers T, Adamo C, Odobel F, Jacquemin D (2012) Through-space charge transfer in rod-like molecules: lessons from theory. J Phys Chem C 116(22):11946–11955
8. Liu J, Zhou D, Wang F, Fabregat-Santiago F, Miralles SG, Jing X, Bisquert J, Wang P (2011) Joint photophysical and electrical analyses on the influence of conjugation order in D-π-A photosensitizers of mesoscopic titania solar cells. J Phys Chem C 115(29):14425–14430
9. Wang C, Li J, Cai S, Ning Z, Zhao D, Zhang Q, Su J-H (2012) Performance improvement of dye-sensitizing solar cell by semi-rigid triarylamine-based donors. Dyes Pig 94(1):40–48
10. Lu M, Liang M, Han H-Y, Sun Z, Xue S (2011) Organic dyes incorporating bis-hexapropyltruxeneamino moiety for efficient dye-sensitized solar cells. J Phys Chem C 15(1):274–281
11. Yu Q-Y, Liao J-Y, Zhou S-M, Shen Y, Liu J-M, Kuang D-B, Su C-Y (2011) Effect of hydrocarbon chain length of disubstituted triphenylamine-based organic dyes on dye-sensitized solar cells. J Phys Chem C 115(44):22002–22008
12. Chai Q, Li W, Zhu S, Zhang Q, Zhu W (2014) Influence of donor configurations on photophysical, electrochemical, and photovoltaic performances in D-π−A organic sensitizers. ACS Sustain Chem Eng 2(2):239–247
13. Farcas A, Tregnago G, Resmerita AM, Dehkordi ST, Cantin S, Goubard F, Aubert PH, Cacialli F (2014) Effect of permodified β−cyclodextrin on the photophysical properties of poly 2,7-(9,9-dioctylfluorene)-alt-(5,5′-bithiophene) main chain polyrotaxanes. J Polym Sci A Polym Chem 52(4):460–471
14. Saleh N, Al-Soud YA, Al-Kaabi L, Ghosh I, Nau WM (2011) A coumarin-based fluorescent PET sensor utilizing supramolecular pK_a shifts. Tetrahedron Lett 52(41):5249–5254
15. Choi H, Kang SO, Ko J, Gao G, Kang HS, Kang M-S, Nazeeruddin MK, Graetzel M (2009) An efficient dye-sensitized solar cell with an organic sensitizer encapsulated in a cyclodextrin cavity. Angew Chem Int Ed 48(32):5938–5941
16. te Velde G, Bickelhaupt FM, Baerends EJ, Guerra CF, Van Gisbergen SJA, Snijders JG, Ziegler T (2001) Chemistry with ADF. J Comput Chem 22(9):931–967
17. Guerra CF, Snijders JG, te Velde G, Baerends EJ (1998) Towards an order-N DFT method. Theor Chem Accounts 99(6):391–403
18. Frisch MJT, Trucks GW, Schlegel HB, Scuseria GE, Robb MA, Cheeseman JR, Montgomery JA, Vreven T, Kudin KN, Burant JC, Millam JM, Iyengar SS, Tomasi J, Barone V, Mennucci B, Cossi M, Scalmani G, Rega N, Petersson GA, Nakatsuji H, Hada M, Ehara M, Toyota K, Fukuda R, Hasegawa J, Ishida M, Nakajima T, Honda Y, Kitao O, Nakai H, Klene M, Li X, Knox JE, Hratchian HP, Cross JB, Bakken V, Adamo C, Jaramillo J, Gomperts R, Stratmann RE, Yazyev O, Austin AJ, Cammi R, Pomelli C, Ochterski JW, Ayala PY, Morokuma K, Voth GA, Salvador P, Dannenberg JJ, Zakrzewski VG, Dapprich S, Daniels AD, Strain MC, Farkas O, Malick DK, Rabuck AD, Raghavachari K, Foresman JB, Ortiz JV, Cui Q, Baboul AG, Clifford S, Cioslowski J, Stefanov BB, Liu G, Liashenko A, Piskorz P, Komaromi I, Martin RL, Fox DJ, Keith T, Al-Laham MA, Peng CY, Nanayakkara A, Challacombe M, Gill PMW, Johnson B, Chen W, Wong MW, Gonzalez C, Pople JA (2009) Gaussian 09. Revision C01 CT Gaussian Inc, Wallingford
19. Becke AD (1993) Density-functional thermochemistry.3. The role of exact exchange. J Chem Phys 98(7):5648–5652
20. Lee CT, Yang WT, Parr RG (1988) Development of the colle-salvetti correlation-energy formula into a functional of the electron-density. Phys Rev B 37(2):785–789
21. Vosko SH, Wilk L, Nusair M (1980) Accurate spin-dependent electron liquid correlation energies for local spin-density calculations-a critical analysis. Can J Phys 58(8):1200–1211
22. Stephens PJ, Devlin FJ, Chabalowski CF, Frisch MJ (1994) Ab-Initio calculation of vibrational absorption and circular-dichroism spectra using density-functional force-fields. J Phys Chem 98(45):11623–11627
23. Yanai T, Tew DP, Handy NC (2004) A new hybrid exchange-correlation functional using the Coulomb-attenuating method (CAM-B3LYP). Chem Phys Lett 393(1–3):51–57
24. Dapprich S, Komaromi I, Byun KS, Morokuma K, Frisch MJ (1999) A new ONIOM implementation in Gaussian98. Part I. The calculation of energies, gradients, vibrational frequencies and electric field derivatives. J Mol Struct 461:1–21
25. Grimme S (2006) Semiempirical GGA-type density functional constructed with a long-range dispersion correction. J Comput Chem 27(15):1787–1799
26. Al-Dmour H, Taylor DM, Cambridge JA (2007) Effect of nanocrystalline-TiO_2 morphology on the performance of polymer heterojunction solar cells. J Phys D Appl Phys 40(17):5034–5038
27. Tian H, Yang X, Pan J, Chen R, Liu M, Zhang Q, Hagfeldt A, Sun L (2008) A Triphenylamine dye model for the study of intramolecular energy transfer and charge transfer in dye-sensitized solar cells. Adv Funct Mater 18(21):3461–3468
28. Koner AL, Nau WM (2007) Cucurbituril encapsulation of fluorescent dyes. Supramol Chem 19(1–2):55–66
29. Nau WM, Mohanty J (2005) Taming fluorescent dyes with cucurbituril. Int J Photoenergy 7(3):133–141
30. Mohanty J, Nau WM (2005) Ultrastable rhodamine with cucurbituril. Angew Chem Int Ed 44(24):3750–3754
31. Ziganshina AY, Ko YH, Jeon WS, Kim K (2004) Stable π-dimer of a tetrathiafulvalene cation radical encapsulated in the cavity of cucurbit[8]uril. Chem Commun 10(7):806–807
32. Haque SA, Park JS, Srinivasarao M, Durrant JR (2004) Molecular-level insulation: an approach to controlling interfacial charge transfer. Adv Mater 16(14):1177–1181
33. Zhang H, Liu L, Gao C, Sun R, Wang Q (2012) Enhancing photostability of cyanine dye by cucurbituril encapsulation. Dyes Pig 94(2):266–270
34. Mohanty J, Pal H, Ray AK, Kumar S, Nau WM (2007) Supramolecular dye laser with cucurbit[7]uril in water. ChemPhysChem 8(1):54–56
35. Clifford JN, Palomares E, Nazeeruddin K, Thampi R, Gratzel M, Durrant JR (2004) Multistep electron transfer processes on dye co-sensitized nanocrystalline TiO_2 films. J Am Chem Soc 126(18):5670–5671
36. Hara K, Sato T, Katoh R, Furube A, Yoshihara T, Murai M, Kurashige M, Ito S, Shinpo A, Suga S, Arakawa H (2005) Novel conjugated organic dyes for efficient dye-sensitized solar cells. Adv Funct Mater 15(2):246–252
37. Mandal AK, Suresh M, Das P, Das A (2012) Restricted conformational flexibility of a triphenylamine derivative on the formation of host-guest complexes with various macrocyclic hosts. Eur J Chem 18(13):3906–3917
38. Cacialli F, Wilson JS, Michels JJ, Daniel C, Silva C, Friend RH, Severin N, Samori P, Rabe JP, O'Connell MJ, Taylor PN, Anderson HL (2002) Cyclodextrin-threaded conjugated polyrotaxanes as insulated molecular wires with reduced interstrand interactions. Nat Mater 1(3):160–164
39. Stanier CA, O'Connell MJ, Clegg W, Anderson HL (2001) Synthesis of fluorescent stilbene and tolan rotaxanes by Suzuki coupling. Chem Commun 5:493–494

40. Willner I, Eichen Y, Willner B (1994) Supramolecular semiconductor receptor assemblies-improved electron-transfer at TiO_2 β-CD colloid interfaces. Res Chem Intermed 20(7):681–700
41. Wu X, Bell TDM, Yeow EKL (2009) Electron transport in the long-range charge-recombination dynamics of single encapsulated dye molecules on TiO_2 nanoparticle films. Angew Chem Int Ed 48(40): 7379–7382
42. Shen P, Liu X, Jiang S, Wang L, Yi L, Ye D, Zhao B, Tan S (2012) Synthesis of new N, N-diphenylhydrazone dyes for solar cells: effects of thiophene-derived pi-conjugated bridge. Dyes Pig 92(3):1042–1051
43. Renouard T, Fallahpour RA, Nazeeruddin MK, Humphry-Baker R, Gorelsky SI, Lever ABP, Gratzel M (2002) Novel ruthenium sensitizers containing functionalized hybrid tetradentate ligands: synthesis, characterization, and INDO/S analysis. Inorg Chem 41(2):367–378